Solid State Communications 254 (2017) 37–41

Contents lists available at ScienceDirect

Solid State Communications

journal homepage: www.elsevier.com/locate/ssc

Communication

Tunable Schottky contacts in the antimonene/graphene van der Waals heterostructures

Wei Li[a], Xinlian Wang[a], Xianqi Dai[b,c,*]

[a] School of Mathematics & Physics, Henan University of Urban Construction, Pingdingshan 467036, China
[b] College of Physics and Materials Science, Henan Normal University, Xinxiang 453007, China
[c] Department of Physics, Zhengzhou Normal University, Zhengzhou, Henan 450044, China

ARTICLE INFO

Communicated by A.H. MacDonald

Keywords:
D. Schottky barrier
B. External electric field
C. Antimonene/graphene vdW heterostructures
D. Electronic structures

ABSTRACT

Electronic structures modulation in the antimonene/graphene van der Waals(vdW) heterostructure with an external electric field(E_{ext}) are investigated by density functional theory calculations. It is demonstrated that weak vdW interactions dominate between antimonene and graphene with their intrinsic electronic properties preserved. Furthermore, the vertical E_{ext} can control not only the Schottky barrier but also the Schottky contacts (*n*-type and *p*-type) and Ohmic contacts (*n*-type) at the antimonene/graphene interface. Meanwhile, the negative E_{ext} can shifts the Dirac point of graphene above the Fermi level, resulting in p-type doping in graphene because electrons can easily transfer from the Dirac point of graphene to the conduction band of antimonene. The present study would open a new avenue for application of ultrathin antimonene/graphene heterostructures in future nano- and optoelectronics.

1. Introduction

Atomically thin two-dimensional (2D) materials are presently being widely investigated owing to their excellent and easily tunable properties, which make them promising candidates for next-generation nanoelectronic and optoelectronic devices [1–17]. The very first material that boosted the research area in 2D materials was grapheme [18,19]. Although graphene has many fascinating properties and has been integrated into different applications, the absence of a bandgap limits its applications in many fields, such as light-emitting diode (LED) [20], solar battery [21] and transistor technology [22]. Very recently, antimonene, which is the monolayer of gray antimony with a rhombohedral structure, has been proposed as a new member of group-V nanosheets. In contrast to the semimetal graphene, antimonene possess a finite bandgap [23,24]. The antimonene nanosheets have a different buckling structure from the monolayer of phosphorus called phosphorene, which prefer to the blue-phosphorus-like structure rather than the black-phosphorus one. Zeng et al. [25] investigated the effects of chemical doping with organic molecules on the electrical properties of the antimonene. The size and edge roughness effects on the thermal properties of antimonene are investigated using the phonon Boltzmann transport method [26]. Meanwhile, the electronic structure of antimonene is also studied by theoretical calculations and characterized by epitaxial growth on Sb_2Te_3 and Bi_2Te_3 substrates [27–29].

The layers of different 2D materials can be stacked to form heterostructures [30–32], which are vertical stacks of 2D layers of dissimilar materials held together by vdW forces, and the novel physical phenomena in such heterostructures have also become a focus of international nanoscience. These vdW heterojuctions show many new properties far beyond individual components. What is more, owing to the weak electron coupling and the lack of dangling bonds at the interface of vdW heterojuctions, their intrinsic electronic properties are preserved without any degradation. In particular, many 2D ultrathin graphene-based vdW heterostructures, have been widely explored theoretically and experimentally, such as graphene/h-BN [33–40], graphene/MoS_2 [41–48], graphene/phosphorene [49–52], graphene/silicone [53–55], graphene/SnS [56], graphene/arsenene [57,58] and graphene/GaSe [59]. Metal/semiconductor is the most common contact types at the interfaces of graphene-based vdW heterojuctions. For the metal/semiconductor interfaces, such as the graphene/MoS_2 heterobilayer, due to the Fermi level pinning, most metals form Schottky contacts to MoS_2 at the metal/MoS_2 interface [60], preventing efficient electron injection/extraction. As a result, the transport properties of metal/MoS_2 heterojuctions are often limited by the contact resistance rather than the intrinsic resistance of the MoS_2 channel. Fortunately, the modulation of the graphene work function, e.g., by an E_{ext}, can be exploited to adjust the grapheme Fermi level to the MoS_2 conduction band minimum to completely remove the Schottky barrier

* Corresponding author at: College of Physics and Materials Science, Henan Normal University, Xinxiang 453007, China.
E-mail address: xqdai@htu.cn (X. Dai).

http://dx.doi.org/10.1016/j.ssc.2017.02.008
Received 9 November 2016; Received in revised form 11 February 2017; Accepted 21 February 2017
Available online 22 February 2017
0038-1098/

at the interface [61]. Supposedly, the use of work-function-tuned graphene electrodes is not limited to MoS_2 but could be used to achieve low resistance contacts to other 2D materials. Therefore, an interesting question arise: whether antimonene and graphene can form a 2D antimonene/graphene vdW heterostructure to obtain some new properties beyond pristine antimonene and graphene? If so, whether E_{ext} for Schottky barrier tuning can also be employed in antimonene /graphene vdW heterostructure?

In the present work, we study the electronic properties of antimonene/graphene vdW heterostructure using first principles calculations, but the main points are the electrically tunable Schottky barriers of antimonene/graphene heterobilayer. The results show that both the properties of antimonene and graphene are preserved upon their contact. Moreover, the E_{ext} can be used to effectively control the Schottky barriers (*n*-type and *p*-type) and contact formation (Schottky and Ohmic contacts) at the antimonene /graphene interface.

2. Models and computational methods

First-principles calculations are based on the density functional theory (DFT) implemented in the VASP package [62]. We adopt the generalized gradient approximation of Perdew, Burke, and Ernzerhof (GGA-PBE) [63] for the exchange correlation functional. The non-bonding van der Waals interaction is incorporated by adding a semi-empirical dispersion potential to the conventional Kohn-Sham DFT energy, through a pair-wise force field following Grimme's DFT-D3 method [64,65]. The projected augmented wave (PAW) potential [66] is employed to describe the electron-ion potential and a kinetic energy cutoff is set to 500 eV. The 2D Brillouin zone integration using the Γ-center scheme is sampled with a 9×9×1 grid for geometry optimization and a 15×15×1 grid for static electronic structure calculations. The convergence for energy is chosen as 10^{-5} eV between two steps. The equilibrium structures are obtained through structural relaxation until Hellmann–Feynman forces are less than 0.01 eV/Å. A vacuum larger than 20 Å is used to eliminate the interaction between adjacent images. The E_{ext} is introduced in the VASP by the dipole layer method with the dipole placed in the vacuum region of the periodic supercell [67]. In order to simulate the antimonene/graphene vdW heterostructure, a 1×1 supercell of antimonene (2 antimony atoms) is obtained as shown in Fig. 1 to match a $\sqrt{3}\times\sqrt{3}$ supercell of graphene (6 carbon atoms) with a negligible lattice mismatch around 1%.

The gray and purple balls represent carbon and antimony atoms, respectively. A vertical E_{ext} is applied perpendicular to the layers. The interlayer distance D between antimonene and graphene is marked.

3. Results and discussion

To quantitatively characterize the interface mechanical properties, we calculated the binding energy of the antimonene/graphene vdW heterostructure. The evolution of the binding energy as a function of the interlayer distance between antimonene and graphene monolayers is shown in Fig. 2. The results indicate that when the interlayer distance is about 4.6 Å, a corresponding binding energy is the lowest, which demonstrates the antimonene/graphene vdW heterojuctions with interlayer distance of 4.6 Å are the most stable. The calculated interlayer distance of 4.6 Å is much larger than the sum of the covalent radii of antimony and carbon atoms, which indicates that weak vdW interactions dominate in the antimonene/grapheme heterobilayer, similar to other 2D vdW graphene-based heterojuctions [68,69].

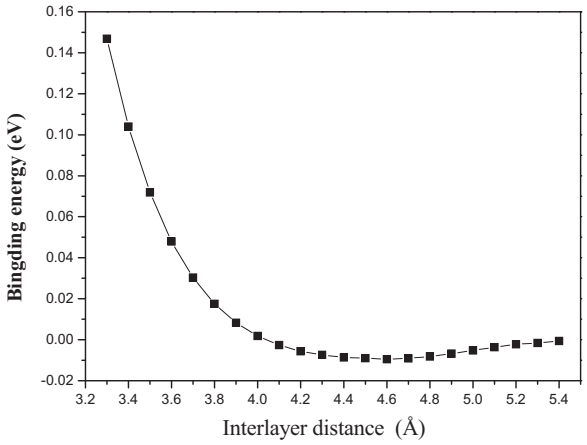

Fig. 2. The binding energy of the antimonene/graphene vdW heterostructures as a function of the interlayer distance.

Electronic structures of pristine antimonene and graphene monolayers are calculated and their band structures are plotted in Fig. 2b and c, respectively. Our results demonstrate that pristine antimonene monolayer is an indirect bandgap semiconductor with a bandgap of 1.24 eV, which is in consistent with previous theoretical calculations [70]. Fig. 3c shows that pristine graphene is no distinguishable bandgap and retains its metallic character, indicating a linear Dirac-like dispersion relation $E(k)= \pm \hbar v_F|k|$ around the Fermi level, where v_F is the Fermi velocity, and the calculated Fermi velocity is about 10^6 m/s at the Dirac point of graphene. Furthermore, compared with the band structures of pristine graphene unit cell, the Dirac cone of the $\sqrt{3}\times\sqrt{3}$ graphene supercell is mapped to the Gamma point. The reason is that the inequivalent K and K' points are folded and coupled into the same Γ-point when a $\sqrt{3}\times\sqrt{3}$ graphene supercell is studied. We then investigate the band structures of antimonene/graphene vdW heterojuction. The projected band structures of antimonene/graphene heterobilayers at the equilibrium interlayer distance are shown in Fig. 3a. Red and blue circles represent the contributions from antimonene and graphene layer, respectively. The weak vdW interaction between antimonene and graphene has little influence on the band structure of the heterojuction. Compared with the band structures of pristine antimonene and graphene shown in Fig. 3b and c, the band structure of the heterostructure is a simple sum of the energy bands of individual

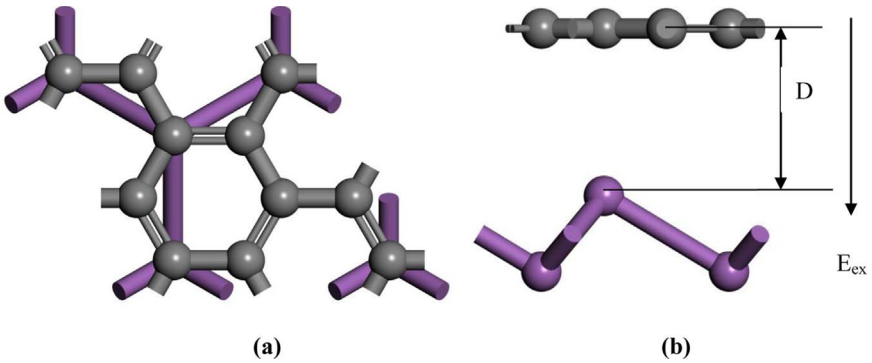

Fig. 1. Top view (a) and side view (b) of the antimonene/graphene vdW heterostructures.

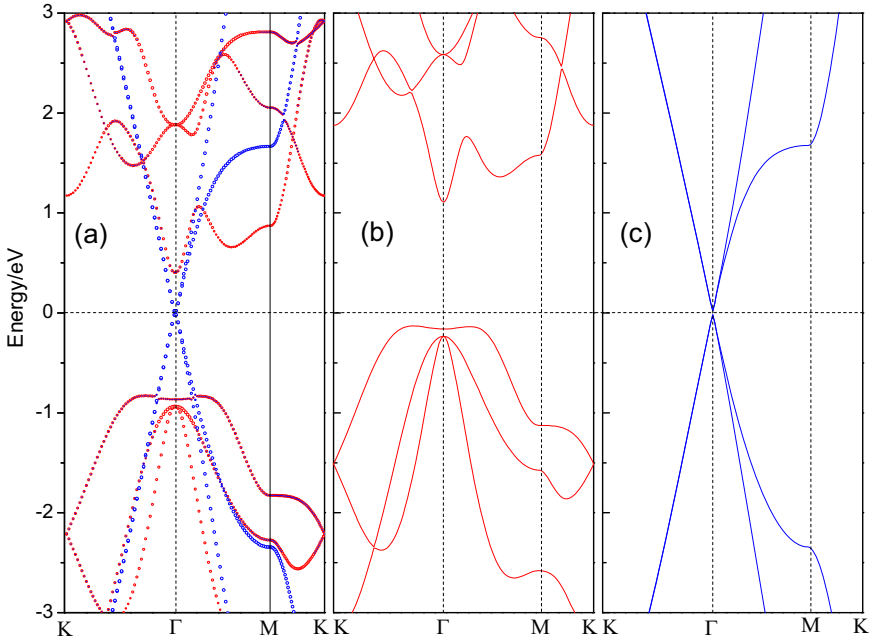

Fig. 3. The projected band structure of (a) antimonene/graphene heterostructure, projection to antimonene layer is denoted by blue circles and to graphene by red circles. Band structures of (b) pristine antimonene and (c) pristine graphene. The Fermi level is set to zero and marked by black dashed lines. (For interpretation of the references to color in this figure legend, the reader is referred to the web version of this article.)

antimonene and graphene. The weak vdW interaction is not enough to modify the morphology of their energy bands. The electronic structures of both antimonene and graphene layers are quite well preserved upon binding. The linear Dirac-like dispersion relationship around the Fermi level of graphene is still preserved in the antimonene/graphene heterobilayer, and the Dirac point of graphene is at the Fermi level. The antimonene layer retains the indirect bandgap semiconductor with a bandgap of 1.22 eV and the graphene layer retains its metallic character. The above results are significant because they show that all properties of the individual materials are conserved, an important behavior for 2D vdW heterojuctions.

The antimonene/graphene configuration is a representative metal-semiconductor contact heterostructure. The Fermi level of the heterostructure lies in the bandgap region of antimonene (Fig. 3a), leading to the formation of a Schottky barrier at the interface, which plays an important role in the device performance. From a device point of view, when using monolayer antimonene as the channel and graphene as the metal contact, the current flow across the metal-semiconductor interface depends on the magnitude of the Schottky barrier height, so it is very important to know its Schottky barrier. The Schottky barrier is an inherent property of the interface and defined via the Schottky–Mott model [46] at the metal-semiconductor interface. If the Fermi level is located above the midgap (CBM+VBM)/2, it is defined as *n*-type Schottky barrier (Φ_{Bn}), where CBM and VBM are the conduction band minimum and the valence band maximum, respectively. Based on the Schottky–Mott model [71], a *n*-type Φ_{Bn} is described as: $\Phi_{Bn}=E_C-E_F$, where E_C and E_F are the CBM and the Fermi level, respectively. On the contrary, If the Fermi level is located below the midgap (CBM+VBM)/2, it is defined as *p*-type Schottky barrier (Φ_{Bp}). A *p*-type Φ_{Bp} is calculated as: $\Phi_{Bp}=E_F-E_V$, where E_F and E_V are the Fermi level and the VBM, respectively. Notice that the sum of both Schottky barriers are approximately equal to the bandgap(E_g) of the semiconductor, namely, $\Phi_{Bn}+\Phi_{Bp}\approx E_g$. Moreover, we find that a *n*-type Schottky contact is formed at the interface with a Schottky barrier height of 0.41 eV, because the work function(4.3 eV) of graphene is close to the electron affinity(4.19 eV) of antimonene.

For the performance of antimonene/graphene based field effect transistors, determination of the effect of E_{ext} on the electronic properties of the antimonene/graphene heterobilayer is important. To explore the influences of E_{ext} on the electronic properties, the projected band structures of the antimonene/graphene vdW heterostructures under different E_{ext} are calculated. In Fig. 4, we show the evolution of the projected band structures of the antimonene/graphene heterobilayer, subjected to an E_{ext} (perpendicular to the heterobilayer). In Fig. 4, with the negative E_{ext} increases from 0 to −1.5 V/nm, the CBM of antimonene is lowered gradually until reduced to below Fermi level. However, with the positive E_{ext} increases from 0 to 1.5 V/nm, the VBM of antimonene is raised gradually, application of a positive E_{ext} makes the VBM of antimonene closer to the Fermi level. Without an E_{ext}, as already pointed out, for antimonene/graphene the CBM is closer to the Fermi level, resulting in a *n*-type Schottky barrier. As shown in Fig. 4, the position of Fermi level moves from the CBM to the VBM of antimonene as the positive E_{ext} increased from 0 to 1.5 V/nm. The magnitude of *n*-type Schottky barrier exceeds *p*-type Schottky barrier gradually. This result shows that a transition from the *n*-type Schottky contact to the *p*-type Schottky contact at the interface occurs when the heterostructure is subjected to a positive E_{ext}. In addition, the negative E_{ext} can moves the Dirac point of graphene above the Fermi level, leading to *p*-type (hole) doping in graphene at the interface as shown in Fig. 4. The reason is that the work function (4.30 eV) of graphene is close to the electron affinity (4.19 eV) of antimonene, therefore the electrons transfer from graphene's Dirac point to antimonene's conduction band under the negative E_{ext}. On the contrary, large positive E_{ext}s are required to make the electrons overcome the bandgap (1.24 eV) of antimonene and then transfer the electrons from antimonene's valence band to graphene's Dirac point. Thus, there is little *n*-type (electron) doping in graphene even when the positive E_{ext} exceeds 1.5 V/nm.

In order to quantitatively characterize the Schottky barrier height and Schottky doping of antimonene/graphene heterostructure, the evolutions of Φ_{Bn}, Φ_{Bp} and $\Phi_{Bn}+\Phi_{Bp}$ of antimonene/graphene heterostructure as a function of E_{ext} have been shown in Fig. 5. With the positive E_{ext} increases from 0 to 1.5 V/nm, the magnitude of Φ_{Bn} gradually increases and the magnitude of Φ_{Bp} gradually decreases. Consequently, the lines of Φ_{Bn} and Φ_{Bp} intersect at 0.45 V/nm, where the Schottky barrier transforms from *n*-type Schottky contact to *p*-type

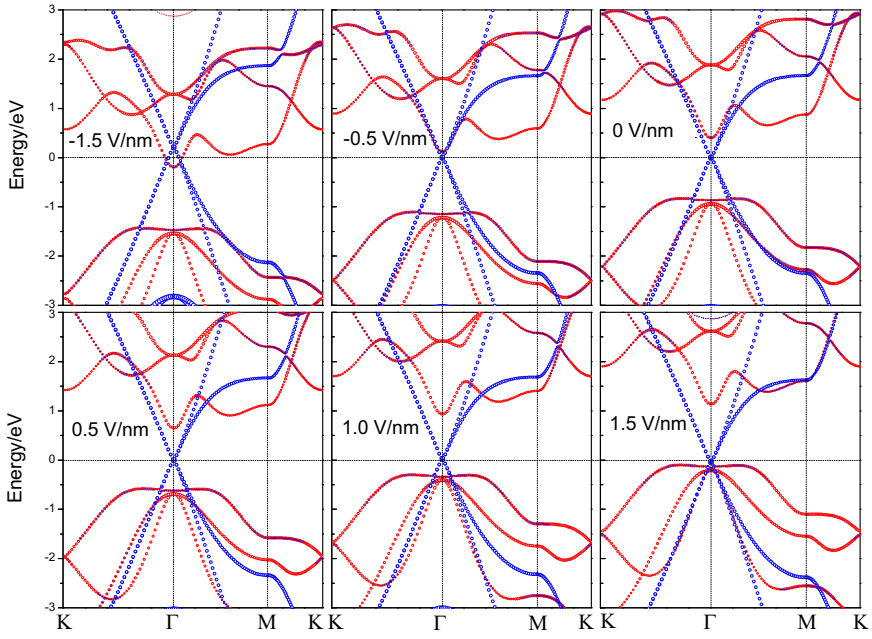

Fig. 4. The projected band structures of the antimonene/graphene vdW heterostructures under different E_{ext}, projection to antimonene layer is denoted by red circles and to graphene by blue circles. (For interpretation of the references to color in this figure legend, the reader is referred to the web version of this article.)

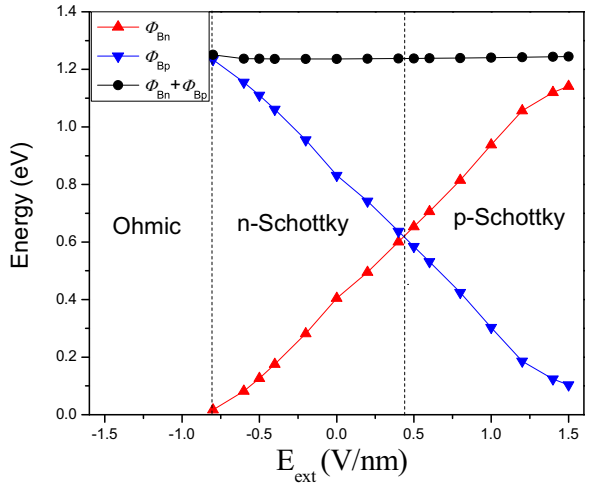

Fig. 5. Schottky barriers Φ_{Bn}, Φ_{Bp} and Φ_{Bn} +Φ_{Bp} in antimonene/graphene vdW heterostructurer as a function of E_{ext}.

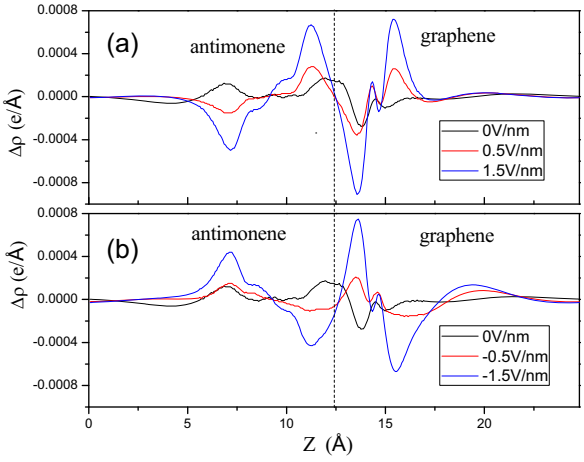

Fig. 6. Plots of the plane-averaged charge density difference along *z* direction under various E_{ext}. The black vertical dashed line denotes the intermediate position of the two monolayers.

Schottky contact. The result demonstrates that not only the Schottky barrier height but also the Schottky contact type can be tuned effectively by the E_{ext} in the antimonene/graphene heterojuction, which may provide a promising route to design tunable Schottky diodes based on the antimonene/graphene vdW heterostructure in the related experimental studies. Under the negative E_{ext} less than −0.8 V/nm, the antimonene/graphene heterojuction interface remains a *n*-type Schottky contact. When the negative E_{ext} increases more than −0.8 V/nm, the *n*-type Schottky contact transforms into the Ohmic contact.

Charge transfer between antimonene and graphene is enhanced as the E_{ext} increases, which may result in the Schottky barrier transition. In order to understand the charge transfer mechanism between antimonene and graphene in the vdW heterojuction, we plot the plane-averaged charge density difference $\Delta\rho(z)$ along the vertical direction to the interface, which can provide a quantitative picture of the charge redistribution at the interface. The plane-averaged charge density difference can be described as $\Delta\rho(z) = \int\rho_{antimonene/graphene}(x, y, z)dxdy - \int\rho_{graphenen}(x, y, z)dxdy - \int\rho_{antimonene}(x, y, z)dxdy$ where $\rho_{antimonene/graphene}(x, y, z)$, $\rho_{graphene}(x, y, z)$ and $\rho_{antimonene}(x, y, z)$ are the plane-averaged charge density at the (x, y, z) point in antimonene/graphene heterostructure, antimonene and graphene monolayer, respectively. As shown in Fig. 6, the plane-averaged charge density differences have been plotted under different E_{ext} of 0 V/nm, 0.5 V/nm, 1.5 V/nm, −0.5 V/nm and −1.5 V/nm, respectively. The results show that the positive and negative E_{ext} have different effects on charge transfer at the interface of antimonene/graphene heterostructure. When applying the positive E_{ext}, more electrons transfer from antimonene to graphene as the E_{ext} increase from 0 to 1.5 V/nm(Fig. 6a), shifting down the Fermi level close to the valence band of antimonene as shown in Fig. 4. Opposite to electrons transfer from antimonene to graphene under the positive E_{ext}, applying E_{ext} along -z direction induces more electrons transfer from graphene to antimonene (Fig. 6b), shifting up the Fermi level close to the conduction band of antimonene as shown in Fig. 4. The amount of charge transfer increase with the strength of E_{ext}, independent of the direction of E_{ext}. More charge transfer between antimonene and graphene indicates a stronger interlayer interaction, resulting in the shift of Fermi level. Therefore, the interfacial

charge transfer and the Fermi level shift are the reasons of the transformation of Schottky barrier from *n*-type Schottky contact to *p*-type Schottky contact and Ohmic contact in the antimonene/graphene heterostructure under different E_{ext}.

4. Conclusions

In conclusion, we have studied the electronic structures of antimonene/graphene vdW heterostructures under different E_{ext} by means of density functional theory calculations. We find that antimonene interacts weakly with graphene via weak vdW interactions and both the intrinsic properties of antimonene and graphene are quite well preserved at the equilibrium interlayer distance. We also show that a *n*-type Schottky contact is formed at the antimonene/graphene vdW heterojuction interface with a Schottky barrier of 0.41 eV. Moreover, the perpendicular E_{ext} can control not only the Schottky barrier but also the Schottky contacts (*n*-type and *p*-type) and Ohmic contacts (*n*-type) at the antimonene/graphene interface. A transition from the *n*-type Schottky contact to the *p*-type Schottky contact occurs at the interface when the positive E_{ext} varies from 0 to 1.5 V/nm. Nevertheless, the *n*-type Schottky barrier transforms into the Ohmic contact as the negative E_{ext} exceeds −0.8 V/nm. In addition, the negative E_{ext} can shift the Dirac point of graphene above the Fermi level, resulting in *p*-type doping in graphene because electrons can easily transfer from the Dirac point of graphene to the conduction band of antimonene. Our work is expected to promote the application of ultrathin antimonene/graphene heterostructure in the next-generation nanoelectronic and photonics devices.

Acknowledgements

We acknowledge support from the National Natural Science Foundation of China (Grant Nos. 61674053, 11504092, U1404109 and 11504334) and the Key Project of Science and Technology Research Program of Henan Educational Committee (Grant No. 15B140008).

References

[1] D. Xiao, G.B. Liu, W.X. Feng, X.D. Xu, W. Yao, Phys. Rev. Lett. 108 (2012) 196802.
[2] Z.Y. Zhu, Y.C. Cheng, U. Schwingenschlogl, Phys. Rev. B 84 (2011) 153402.
[3] Q.H. Wang, K. Kalantar-Zadeh, A. Kis, J.N. Coleman, M.S. Strano, Nat. Nanotechnol. 7 (2012) 699.
[4] J.N. Coleman, M. Lotya, A. O'Neill, S.D. Bergin, P.J. King, U. Khan, K. Young, A. Gaucher, S. De, R.J. Smith, I.V. Shvets, S.K. Arora, G. Stanton, H.Y. Kim, K. Lee, G.T. Kim, G.S. Duesberg, T. Hallam, J.J. Boland, J.J. Wang, J.F. Donegan, J.C. Grunlan, G. Moriarty, A. Shmeliov, R.J. Nicholls, J.M. Perkins, E.M. Grieveson, K. Theuwissen, D.W. McComb, P.D. Nellist, V. Nicolosi, Science 331 (2011) 568.
[5] H. Shu, P. Luo, P. Liang, D. Cao, X. Chen, Acs Appl. Mater. Inter 7 (2015), 2015, p. 7534.
[6] D. Cao, T. Shen, P. Liang, X. Chen, H. Shu, J. Phys. Chem. C 119 (2015) 4294.
[7] H. Shu, F. Li, C. Hu, P. Liang, D. Cao, X. Chen, Nanoscale 8 (2016) 2918.
[8] C. Fan, Z.M. Wei, S.X. Yang, J.B. Li, RSC Adv. 4 (2014) 775.
[9] S.J. Liu, N.J. Huo, S. Gan, Y. Li, Z.M. Wei, B.J. Huang, J. Liu, J.B. Li, H.D. Chen, J. Mater. Chem. C 3 (2015) 10974.
[10] C. Fan, Y. Li, F.Y. Lu, H.X. Deng, Z.M. Wei, J.B. Li, RSC Adv. 6 (2016) 422.
[11] X.T. Wang, L. Huang, X.W. Jiang, Y. Li, Z.M. Wei, J.B. Li, J. Mater. Chem. C 4 (2016) 3143.
[12] M.Z. Zhong, L. Huang, H.X. Deng, X.T. Wang, B. Li, Z.M. Wei, J.B. Li, J. Mater. Chem. C 4 (2016) 6492.
[13] C.X. Xia, Y.T. Peng, H. Zhang, T.X. Wang, S.Y. Wei, Y. Jia, Phys. Chem. Chem. Phys. 16 (2014) 19674.
[14] W.Q. Xiong, C.X. Xia, T.X. Wang, J. Du, Y.T. Peng, X. Zhao, Y. Jia, Phys. Chem. Chem. Phys. 18 (2016) 28759.
[15] H. Zhang, C.X. Xia, X. Zhao, T.X. Wang, J.B. Li, Appl. Surf. Sci. 356 (2015) 1200.
[16] Y. Li, C.X. Xia, T.X. Wang, X.M. Tan, X. Zhao, S.Y. Wei, Solid. State Commun. 230 (2016) 6.
[17] J. Du, C.X. Xia, T.X. Wang, X. Zhao, X.M. Tan, S.Y. Wei, Appl. Surf. Sci. 378 (2016) 350.
[18] K.S. Novoselov, A.K. Geim, S.V. Morozov, D. Jiang, Y. Zhang, S.V. Dubonos, I.V. Grigorieva, A.A. Firsov, Science 306 (2004) 666.
[19] A.K. Geim, K.S. Novoselov, Nat. Mater. 6 (2007) 183.
[20] G. Liu, J. Zhang, C. Tan, N. Tansu, IEEE Photonics J. 5 (2013) 2201011.
[21] D. Mariotti, S. Mitra, V. Svrcek, Nanoscale 5 (2013) 1385.
[22] Y. Zhang, T. Tang, C. Girit, Z. Hao, M.C. Martin, A. Zettl, M.F. Crommie, Y. Shen, F. Wang, Nature 459 (2009) 820.
[23] S. Zhang, Z. Yan, Y. Li, Z. Chen, H. Zeng, Angew. Chem. 127 (2015) 3155.
[24] S. Zhang, M. Xie, F. Li, Z. Yan, Y. Li, E. Kan, W. Liu, Z. Chen, H. Zeng, Angew. Chem. Int. Ed. 55 (2016) 1666.
[25] M.Q. Xie, S.L. Zhang, B. Cai, Y.S. Zou, H.B. Zeng, RSC Adv. 6 (2016) 14620.
[26] K.G. Sanjeev, S. Yogesh, G.X. Wang, R. Pandey, Chem. Phys. Lett. 641 (2015) 169.
[27] G. Wang, R. Pandey, S.P. Karna, ACS Appl. Mater. Interfaces 7 (2015) 11490.
[28] M. Zhao, X. Zhang, L. Li, Sci. Rep. 5 (2015) 16108.
[29] T. Lei, C. Liu, J.L. Zhao, J.M. Li, Y.P. Li, J.O. Wang, R. Wu, H.J. Qian, H.Q. Wang, K. Ibrahim, J. Appl. Phys. 119 (2016) 015302.
[30] C. Wang, S.X. Yang, W.Q. Xiong, C.X. Xia, H. Cai, B. Chen, X.T. Wang, X.Z. Zhang, Z.M. Wei, S. Tongay, J.B. Li, Q. Liu, Phys. Chem. Chem. Phys. 18 (2016) 27750.
[31] L. Huang, Y. Li, Z.M. Wei, J.B. Li, Sci. Rep. 5 (2015) 16448.
[32] L. Huang, N.J. Huo, Y. Li, H. Chen, J.H. Yang, Z.M. Wei, J.B. Li, S.S. Li, J. Phys. Chem. Lett. 6 (2015) 2483.
[33] G. Giovannetti, P.A. Khomyakov, G. Brocks, P.J. Kelly, J. van den Brink, Phys. Rev. B 76 (2007) 073103.
[34] C.R. Dean, A.F. Young, I. Meric, C. Lee, L. Wang, S. Sorgenfrei, K. Watanabe, T. Taniguchi, P. Kim, K.L. Shepard, J. Hone, Nat. Nanotechnol. 5 (2010) 722.
[35] J. Xue, J. Sanchez-Yamagishi, D. Bulmash, P. Jacquod, A. Deshpande, K. Watanabe, T. Taniguchi, P. Jarillo-Herrero, B.J. LeRoy, Nat. Mater. 10 (2011) 282.
[36] E. Kan, H. Ren, F. Wu, Z. Li, R. Lu, C. Xiao, K. Deng, J. Yang, J. Phys. Chem. C 116 (2012) 3142.
[37] R. Balu, X. Zhong, R. Pandey, S.P. Karna, Appl. Phys. Lett. 100 (2012) 052104.
[38] M.X. Liu, Y.C. Li, P.C. Chen, J.Y. Sun, D.L. Ma, Q.C. Li, T. Gao, Y.B. Gao, Z.H. Cheng, X.H. Qiu, Y. Fang, Y.F. Zhang, Z.F. Liu, Nano Lett. 14 (2014) 6342.
[39] Y.D. Gao, R.J. Shiue, X.T. Gan, L.Z. Li, C. Peng, I. Meric, L. Wang, A. Szep, D.W. Jr, J. Hone, D. Englund, Nano Lett. 15 (2015) 2001.
[40] S. Byun, J.H. Kim, S.H. Song, M. Lee, J.J. Park, G. Lee, S.H. Hong, D.J. Lee, Chem. Mater. 28 (2016) 7750.
[41] L. Britnell, R.V. Gorbachev, R. Jalil, B.D. Belle, F. Schedin, A. Mishchenko, T. Georgiou, M.I. Katsnelson, L. Eaves, S.V. Morozov, N.M.R. Peres, J. Leist, A.K. Geim, K.S. Novoselov, L.A. Ponomarenko, Science 335 (2012) 947.
[42] L. Britnell, R.M. Ribeiro, A. Eckmann, R. Jalil, B.D. Belle, A. Mishchenko, Y.-J. Kim, R.V. Gorbachev, T. Georgiou, S.V. Morozov, A.N. Grigorenko, A.K. Geim, C. Casiraghi, A.H. Castro Neto, K.S. Novoselov, Science 340 (2013) 1311.
[43] W.J. Yu, Z. Li, H. Zhou, Y. Chen, Y. Wang, Y. Huang, X. Duan, Nat. Mater. 12 (2013) 246.
[44] M.S. Choi, G.H. Lee, Y.J. Yu, D.Y. Lee, S.H. Lee, P. Kim, J. Hone, W.J. Yoo, Nat. Commun. 4 (2013) 1624.
[45] K. Roy, M. Padmanabhan, S. Goswami, T.P. Sai, G. Ramalingam, S. Raghavan, A. Ghosh, Nat. Nanotechnol. 8 (2013) 826.
[46] C.Y. Zhao, X. Wang, J.H. Kong, J.M. Ang, P.S. Lee, Z.L. Liu, X.H. Lu, ACS Appl. Mater. Interfaces 8 (2016), 2016, p. 2372.
[47] C.J. Shih, Q.H. Wang, Y. Son, Z. Jin, Dl Blankschtein, M.S. Strano, ACS Nano 8 (2014) 5790.
[48] N.J. Huo, Z.M. Wei, X.Q. Meng, J. Kang, F.M. Wu, S.S. Li, S.H. Wei, J.B. Li, J. Mater. Chem. C 3 (2015) 5467.
[49] W. Hu, T. Wang, J. Yang, J. Mater. Chem. C 18 (2015) 4756.
[50] J.E. Padilha, A. Fazzio, A.J.R. da Silva, Phys. Rev. Lett. 114 (2015) 066803.
[51] A. Avsar, I.J. Vera-Marun, J.Y. Tan, K. Watanabe, T. Taniguchi, A.H.C. Neto, O. Barbaros, ACS Nano 9 (2015) 4138.
[52] G.C. Guo, D. Wang, X.L. Wei, Q. Zhang, H. Liu, W.M. Lau, L.M. Liu, J. Phys. Chem. Lett. 6 (2015) 5002.
[53] W. Hu, Z. Li, J. Yang, J. Chem. Phys. 139 (2013) 154704.
[54] Y. Cai, C.P. Chuu, C.M. Wei, M.Y. Chou, Phys. Rev. B 88 (2013) 245408.
[55] B. Liu, J.A. Baimova, C.D. Reddy, A.W.K. Law, S.V. Dmitriev, H. Wu, K. Zhou, ACS Appl. Mater. Interfaces 6 (2014) 18180.
[56] W.Q. Xiong, C.X. Xia, X. Zhao, T.X. Wang, Y. Jia, Carbon 109 (2016) 737.
[57] C.X. Xia, B. Xue, T.X. Wang, Y.T. Peng, Y. Jia, Appl. Phys. Lett. 107 (2015) 193107.
[58] W. Li, T.X. Wang, X.Q. Dai, X.L. Wang, Y.Q. Ma, S.S. Chang, Y.N. Tang, Physica E 88 (2017) 6.
[59] Z.B. Aziza, H. Henck, D. Pierucci, M.G. Silly, E. Lhuillier, G. Patriarche, F. Sirotti, M. Eddrief, A. Ouerghi, ACS Nano 10 (2016) 9679.
[60] C. Gong, L. Colombo, R.M. Wallace, K. Cho, Nano Lett. 14 (2014) 1714.
[61] L.L. Yu, Y.H. Lee, X. Ling, E.J.G. Santos, Y.C. Shin, Y.X. Lin, M. Dubey, E. Kaxiras, J. Kong, H. Wang, T. Palacios, Nano Lett. 14 (2014) 3055.
[62] G. Kresse, J. Hafner, Phys. Rev. B 47 (1993) 558.
[63] J.P. Perdew, K. Burke, M. Ernzerhof, Phys. Rev. Lett. 77 (1996) 3865.
[64] S. Grimme, J. Antony, S. Ehrlich, S. Krieg, J. Chem. Phys. 132 (2010) 154104.
[65] S. Grimme, S. Ehrlich, L. Goerigk, J. Comp. Chem. 32 (2011) 1456.
[66] P.E. Blochl, Phys. Rev. B 50 (1994) 17953.
[67] J. Neugebauer, M. Scheffler, Phys. Rev. B 46 (1992) 16067.
[68] G. Giovannetti, P.A. Khomyakov, G. Brocks, P.J. Kelly, J. van den Brink, Phys. Rev. B 76 (2007) 073103.
[69] A. Du, S. Sanvito, Z. Li, D. Wang, Y. Jiao, T. Liao, A. Sun, Y.H. Ng, Z. Zhu, R. Amal, S.C. Smith, J. Am. Chem. Soc. 134 (2012) 4393.
[70] A.C. Ferrari, J.C. Meyer, V. Scardaci, C. Casiraghi, M. Lazzeri, F. Mauri, S. Piscanec, D. Jiang, K.S. Novoselov, S. Roth, A.K. Geim, Phys. Rev. Lett. 97 (2006) 187401.
[71] J. Bardeen, Phys. Rev. 71 (1947) 717.